Altmeyer, J.; Suhuddin, U.F.H.; dos Santos, J.F.; Amancio-Filho, S.T.:

Microstructure and mechanical performance of metal-composite hybrid joints produced by FricRiveting

In: Composites / B (2015) Elsevier

DOI: 10.1016/j.compositesb.2015.06.015

Microstructure and mechanical performance of metal-composite hybrid joints produced by FricRiveting

J. Altmeyer[a,b,*], U. Suhuddin[a], J.F. dos Santos[a], S.T. Amancio-Filho[a,b,]

[a] *Helmholtz-Zentrum Geesthacht GmbH, Institute of Materials Research, Materials Mechanics, Solid State Joining Processes, Geesthacht, Germany*
[b] *Helmholtz-Zentrum Geesthacht GmbH, Institute of Materials Research, Materials Mechanics, Solid State Joining Processes, Advanced Polymer-Metal Hybrid Structures Group, Geesthacht, Germany*

Abstract

The mechanical performance and microstructure of friction riveted metallic-insert joints made of polyether ether ketone (PEEK) composite reinforced with 30 % short carbon fibers and grade 3 titanium was studied. The metallic-insert joints reached a maximal pull-out tensile force of 10.6 kN, which corresponds to 100 % of the titanium base material strength. The dimensions of the deformed metallic rivet were correlated with the mechanical pull-out performance of the joint. It was shown the pull-out force increased as the rivet tip widened. Microstructural analyses of the metallic part of the joint revealed the presence of different microstructural zones: a friction zone, and two thermomechanically affected zones 1 and 2. It is believed that frictional heat during the process was mainly generated by the friction between the tip of the rivet and the composite substrate in the friction zone. Based on the thermally introduced changes and fiber orientation, the metallic-insert joint was categorized into three different zones in the composite part of the joint - the stir zone, a thermomechanically affected zone and a heat-affected zone. A study of the material flow showed that the flow of the composite was strongly affected by the rotation and axial movement of the rivet.

*Corresponding author
Email addresses: julie.altmeyer@hzg.de (J. Altmeyer), uceu.suhuddin@hzg.de (U. Suhudin), jorge.dos.santos@hzg.de (J.F. dos Santos), sergio.amancio@hzg.de (S.T. Amancio-Filho)

1. Introduction

In recent years, the use of thermoplastics with and without fiber reinforcement has increased significantly in the transportation industry, such as in automotive and aircraft structures or in other high-performance engineering applications, including wind-energy structures, sporting goods and medical appliances [1]. One of the main reasons for moving from purely metallic structures toward composite multimaterial structures is the possibility of tailoring their performance to the structural requirements [2, 3].

Using thermoplastic composites gives the advantages of their high fracture toughness, better environmental resistance and recyclability [1, 4, 2]. The increasing presence of thermoplastic parts in large structural components requires adequate joining techniques for multimaterial structures [5]. Currently, thermoplastics and reinforced thermoplastics can be joined using three main groups of techniques: mechanical fastening, adhesive bonding and welding [5, 6, 7, 8, 9]. The design of large, complex structures incorporating new materials generates new combinations of materials requiring new joining technologies [3, 10].

Some recent and less-explored joining technologies have become available for joining thermoplastic composites, such as induction- and resistance welding or laser bonding. These technologies make use of the properties of the thermoplastic matrices which are repeatedly reheated or remelted and consolidated [11, 12, 13].

One alternative joining technology is friction riveting (FricRiveting), a friction-based, spot-joining process developed for joining thermoplastics to lightweight alloy structures, first patented by Helmholtz-Zentrum Geesthacht [14, 15]. FricRiveting bridges the gap between mechanical fastening and welding, offering advantages that include short joining cycles and limited surface pretreatment of the joint components. The method also reduces the number of installation steps by eliminating predrilling [16].

One example of the FricRiveting process is in the production of friction-riveted metallic-insert joints consisting of a metal rivet anchored inside a thermoplastic base plate. This process was introduced by Amancio-Filho [17], where the friction riveting process was investigated using unreinforced polyetherimide (PEI) and aluminum 2024. The main steps in the process are described in Figure 1. First, the rivet begins to rotate, moving toward the thermoplastic base plate and finally touching it (see Figure 1 b). The combination of rotation and axial pressure generates frictional heat, forming a thin layer of molten polymer around the tip of the rivet. Because the rivet is continuously fed during the friction phase, molten material is partially expelled, forming a flash. The heat generation rate during this phase increases, and the heat input increases until it exceeds the heat outflow, due to the extremely low thermal conductivity of the polymer substrate. As a result of the local increase in temperature, the rivet tip becomes plasticized. At this point, the motor brake is activated, decelerating the spindle rotation; an additional pressure (the forging pressure, FoP) is applied (Figure 1 c). The molten polymer layer below the rivet tip is suppressed by the additional axial pressure, and the tip of the rivet is forged backwards by the revealed solid region, widening the rivet tip and creating an inverted parabolic or mushroom-like shape. During the last step (Figure 1 d) the joint consolidates and cools while subjected to constant external pressure. The rivet remains strongly anchored inside the polymeric substrate, forming a metallic-insert joint.

Figure 2 is a monitoring diagram of a friction riveted joint, including the main process parameters and variables. The figure shows three separate process steps: the friction step, forging step and consolidation. In the friction step, the rivet begins to penetrate the composite substrate with the preset process parameters, leading to a time-dependent increase in torque and axial displacement. In the forging step, the axial force is increased and the rotation is decreased, leading to an intermediate rise in torque and axial displacement. During the consolidation step the joint cools and the rivet reaches its final strength as the axial pressure is reduced.

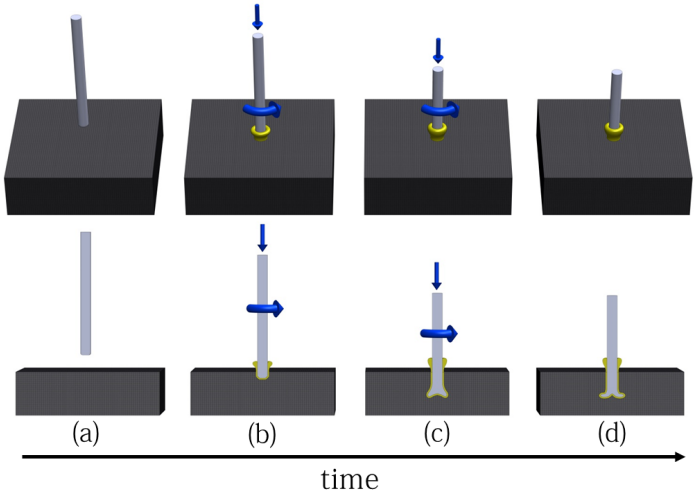

Figure 1: Friction riveting process steps: (a) Positioning of joining parts. (b) Frictional heat creates a molten polymer layer, and the rivet penetrates the polymer. (c) Axial force on the rivet is increased, resulting in anchoring by widening (mushrooming) the rivet tip. (d) Consolidation of the joint

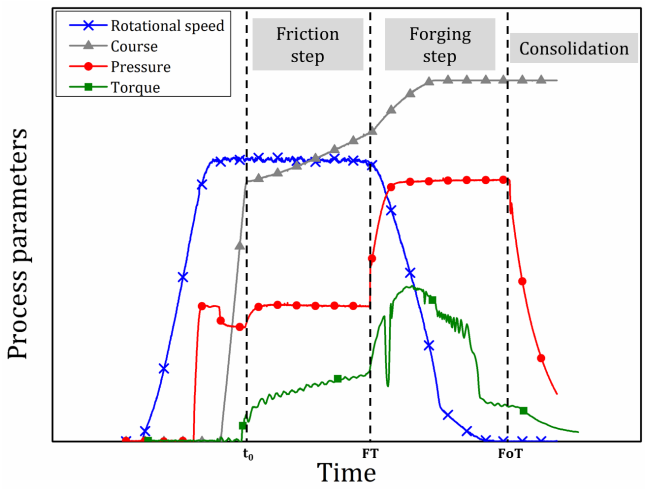

Figure 2: Typical evolution of friction riveting process parameters over time

The mechanical performance of friction-riveted metallic-insert joints has been discussed in earlier studies [18, 19]. Amancio-Filho [18] investigated metallic-insert joints of polyetherimide and aluminum 2024 which produced an ultimate tensile force of 6.1 kN, which was 93 % of the tensile strength of the rivet base material. Joints failed in "through the rivet" mode at its base material, outside the joined area. Blaga et al. [19] studied the tensile pull-out behaviour of metallic-insert joints of glass fibre reinforced polyetherimide and grade 2 titanium. They found that the joints produced a good mechanical performance, achieving an ultimate tensile force of up to 4 kN, at which point they failed in "full rivet pull-out" mode.

In previous studies of friction-riveted joints made of PEI and aluminum 2024, Amancio-Filho [17, 18] identified five different microstructural zones in the joint: the polymer heat-affected zone (PHAZ), the polymer thermomechanically affected zone (PTMAZ), the metal heat-affected zone (MHAZ), the metal thermomechanically affected zone (MTMAZ) and the anchoring zone (AZ). This classification was based on a careful analysis using an optical microscope. These studies indicated, however, that a higher-resolution analysis would further clarify the nature of the observed microstructures [17, 18].

In the present work, grade 3 titanium was joined to polyether ether ketone (PEEK) by the FricRiveting process. The pull-out performance of the friction-riveted metallic-insert joints was correlated with the shape and size of the anchoring feature inside the PEEK composite structure. The microstructural zones in the composite and in the metallic regions of the joint were also identified and characterized using also a scanning electron microscope. The zones in the composite were identified from the porosity and the orientation of the fibers. The microstructural zones in the metallic component were identified by grain size and the fraction of high-angle boundaries (HABs). The results of these analyses are discussed below, taking into consideration the microstructural classification proposed by Amancio-Filho [17, 18].

2. Experimental

The metallic insert joints were made from two parts: a short-fiber-reinforced polymeric base plate and a metallic rivet. The thermoplastic composite substrate material was PEEK reinforced with 30 % wt short carbon fibers (Ketron® PEEK CA30, Arthur Krueger, Barsbuettel, Germany). The base plate geometry and dimensions were 70 mm × 70 mm × 21 mm. PEEK is a high-performance, semi-crystalline thermoplastic polymer [20, 21, 22, 23]; short carbon-fiber-reinforced PEEK is often selected for its excellent wear resistance and good mechanical performance at elevated temperatures [23]. Figure 3 a shows the microstructure of the polymeric base plates. The relevant properties of the PEEK composite used for this work are listed in table 1. This composite is used in the aerospace, automotive, chemical and medical industries [21, 23].

The rivets were made from commercially pure grade 3 titanium rods. They were 60 mm long with a diameter of 5 mm. An EBSD map of the microstructure of the titanium base material is shown in Figure 3 b. Grade 3 titanium contains only the alpha phase. Figure 3 b shows the microstructure parallel to the extrusion direction, displaying equiaxed alpha grains. This grade of commercially pure titanium is often used for its excellent corrosion resistance and reasonably good strength-to-weight ratio. It is often used to bridge the design gap between aluminum and steel [28]. The relevant properties of this alloy are given in Table 1. The chemical composition of the rivet material is 0.07 % C, 0.0001 %

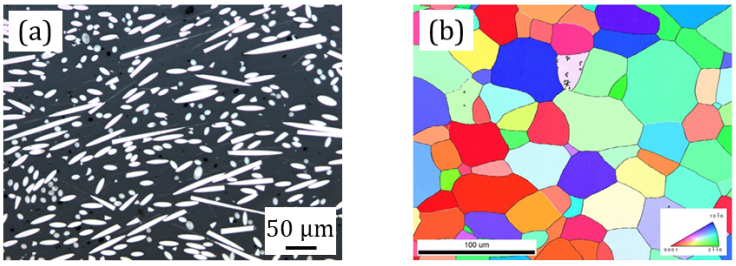

Figure 3: Joint components: (a) LOM picture of Ketron® PEEK CA30; (b) EBSD map of the microstructure of the grade 3 titanium base material, showing the equiaxed alpha-grains

Table 1: Main properties of the short carbon-fiber-reinforced PEEK base material [2, 24, 25, 26, 27, 23, 22] and grade 3 titanium base material [28, 29, 30]

	PEEK-CA30	Ti grade 3
Tensile strength	130 MPa	545 MPa
Tensile modulus	7.7 GPa	105 GPa
Hardness	35 HV 0.1	235 HV 0.1
Thermal conductivity	0.92 W/m K	19.9 W/m K
Melting temperature	334 °C	1660 °C
Glass transition temperature	143 °C	

H, 0.17 % O, 0.01 % N, 0.05 % Fe and balanced with Ti. Commercially pure titanium is typically used in non-structural aircraft parts and for engineering applications requiring corrosion resistance [28].

The joining equipment used for sample manufacture was a high-speed friction welding system (RSM 400; Harms & Wende GmbH). The RSM 400 has a maximum rotational speed of 23000rpm, a nominal power of 1.8 kW and a maximum axial force of 6 kN (corresponding to a manometric machine pressure of 10bar and 1 MPa). In the present investigation, the rotational speed (RS) ranged from 18 000 to 20000rpm, friction time (FT) was between 1 and 1.5 s, friction pressure ranged from 0 to 0.8 MPa, forging pressure from 0.9 to 1 MPa, and the forging time was maintained at a constant 10 s, both to allow consolidation under defined pressure and to avoid shrinkage. The parameter combinations used in the present investigation are given in Table 2. Three replicas were produced for each parameter combination. An example of the friction-riveted metallic-insert joint is shown in Figure 4 a. The torque associated with rivet rotation and insertion was determined by a customized torque measurement platform using a piezoelectric sensor with load amplification, and was then used to calculate the mechanical energy input.

The temperature evolution due to the FricRiveting process was measured by an infrared (IR) thermography system consisting of an IR thermocamera, (ImageIR®8300, Infratech GmbH, Germany) and a computer for data acquisition and analysis using IRBIS® 3 Professional software. The distance from the

Table 2: Process parameter configurations

Configuration	Process settings			
	RS [rpm]	FT [s]	FP [MPa]	FoP [MPa]
1	18 000	1	0.7	0.9
2	18 000	1	0.7	1
3	18 000	1.5	0.7	1
4	20 000	1	0.7	0.9
5	20 000	1.5	0.8	1

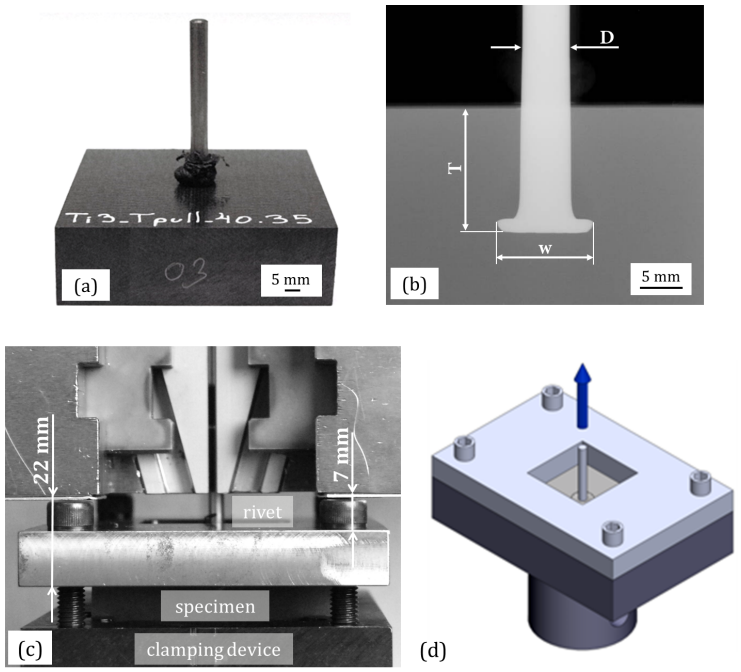

Figure 4: (a) Photograph of a friction-riveted metallic-insert joint. (b) X-ray image of a metallic-insert joint, indicating initial diameter of the rivet (D), penetration depth (T) and widening of rivet tip (w). Clamping device for pull-out testing. (c) Test set-up, showing active components and free clamping length. (d) Schematic 3D view of clamping device

object lens to the touch-down region of the rivet was 321 mm. Measurement was conducted at an incidence angle of 45°. The data acquisition rate was set to 80 Hz, and temperature calibration ranged between 150 and 600 °C.

Temperature evolution was measured from the point at which the expelled material began to accumulate around the rivet in the joining process. It was assumed that the low thermal conductivity of the polymer would ensure that the average temperature of the expelled (flash) material was very similar to that of the molten polymer layer around the plasticized rivet tip inside the polymer base plate [17, 31, 18].

X-ray radiography was performed for precise measurement of the rivet penetration depth (T) and the widening of the rivet tip (w) in accordance with the EN 1435 standard [32], using a Seifert Isovolt 320/13 (tube voltage 60 kV; tube current 3.7 mA). All joints were subjected to X-ray scanning before mechanical testing to investigate the relationship between the size and shape of the anchoring feature and its mechanical performance, since X-ray scans reveal the exact dimensions of the anchoring zone at the center of the joints. An example indicating the measurement positions is shown in Figure 4 b.

Pull-out tests were conducted to assess the global mechanical strength of the metallic-insert joints. Tests were performed at room temperature using a Zwick/Roell 1478 testing machine with a load range up to 100 kN in accordance with EN 2591 [33]. The tensile force and displacement were monitored during displacement-controlled static loading at 1 mm/min. The clamping device shown in Figure 4 c and d was specially designed to ensure a uniform stress distribution in the composite base plate during the tensile test. The free rivet tip was clamped inside the gripping jaws.

For microstructure analyses, the samples were sectioned across the center of the rivet, then ground and polished with an OPS solution modified to contain 20 % hydrogen peroxide and 5 % ammonia. For light optical microscopy (LOM), the samples were etched with a modified Weck's reagent (100 mL distilled water, 25 mL ethanol and 2 g ammonium bifluoride) which showed the alpha grains and twins colored according to their orientation [34]. For electron backscatter

diffraction (EBSD) analysis, the samples were electropolished using A3 solution at a voltage of 60 V for 20 s at 10 °C [35].

The prepared specimens were analysed with a Leica DM 15000 M LOM and a FEI Quanta 650 field emission gun scanning electron microscope equipped with a EDAX Hikari XP EBSD camera operated at 30 kV. The EBSD maps measure 120 µm × 120 µm and 270 µm × 270 µm in 0.3 µm steps. The average confidence index varied between 0.22 and 0.68. The quality of EBSD data is comparable to face-centered cubic (fcc) metals, for which it has been shown that the fraction of correctly indexed patterns with confidence indices greater than 0.1 is 95 % (TSL OIM help). To eliminate false boundaries resulting from orientation noise, the lower limit of boundary misorientation was set at 2°. Misorientations between 2 and 15° were defined as low-angle boundaries (LABs), and above 15° as high-angle boundaries (HABs). LABs and HABs are depicted in the EBSD maps as gray and black lines respectively. Twin boundaries are indicated by red lines. All grain-size measurements were made on the EBSD maps by the linear intercept length method.

3. Results and discussion

3.1. Mechanical performance of the joints

All the configurations shown in Table 2 were successfully riveted; no unusual circumstances, such as the development of smoke or ash, were observed during the process.

The average pull-out force for all of the configurations including the standard deviation, shown in Table 3, ranged from 6.3 kN to 10.6 kN. The table also shows that two types of failure mode were observed, depending on the parameter configuration. The specimens in configurations 1 to 4 failed by mode III ("full rivet pull-out") and those in configuration 5 failed in failure mode I ("through the rivet"). Figure 5 a and b show an example of each failure mode. These types of failure had previously been observed and discussed by Amancio-Filho et al. [36], Blaga et al. [19] and Altmeyer et al. [37]. In failure type I, ductile fracture in the rivet occurs outside the anchoring zone. This type of failure is the

favored one, since it occurs due to high tensile forces at failure, which usually correspond to the ultimate tensile strength of the rivet base material. Failure mode III occurs when the rivet tip has been deformed by only a relatively small amount, leading to its reduced mechanical anchoring inside the substrate. A crack initiates around the anchoring zone and finally leads to a complete pull-out of the rivet, leaving a hole of diameter similar to that of the deformed rivet tip. This type of failure occurs at a relatively low tensile force.

Figure 5şhows an example of the recorded force-displacement curves for both failure modes and for the grade 3 titanium base material rivet. It is seen that the force-displacement curve of the titanium rivet and the failure of the joint in mode I are similar, due to the similar failure behaviors of the rivet and the joint. In both specimens, extensive plastic deformation (necking) was observed when subjected to tensile loading, until they finally failed. It is believed that, in case of the joints failing in failure mode I, the widening of the rivet tip inside the composite substrate is large enough to behave in a similar way to the clamping of the rivet by the gripping jaws of the testing machine. Therefore, ductile metallic failure occurs in the middle of the free length of the rivet between the anchoring zone inside the composite (metallic-insert joint region acting as clamping device) and the rivet tip clamped in the gripping jaw. The curve representing the joint failing in mode III initially shows elastic deformation (slope of the force-displacement curve) similar to the curve of the specimen failing in mode I, but peaks at a much lower load. The load then gradually decreases as the anchored rivet is pulled out from the composite substrate.

The deformation widths and the penetration depths measured from the X-ray radiography scans are summarized in Table 3. This shows that the penetration depth ranges between 7.4 and 12.9 mm and the widening of the rivet tip between 6.7 and 9.5 mm. An example of the X-ray scans is shown in Figure 4 b. To describe the relationship between the geometry of the deformed rivet inside the composite substrate and the mechanical performance of the metallic-insert joint, the concept of "mushrooming efficiency" (e_{much}) was introduced by Altmeyer et al. [37]. The mushrooming efficiency combines the initial rivet

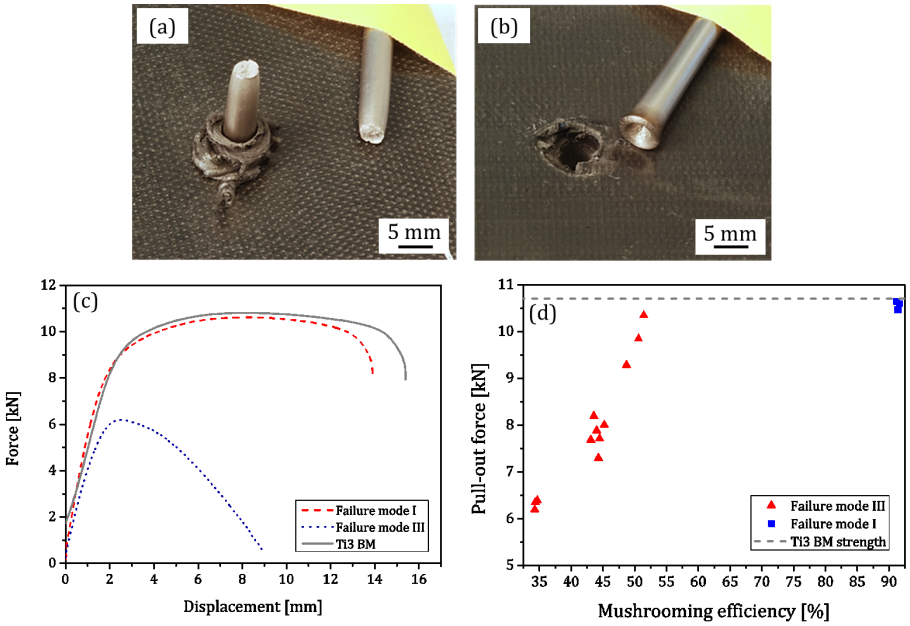

Figure 5: Failure modes of the metallic-insert joints: (a) "Through the rivet" (rivet failure in the Ti base material, failure mode I). (b) "Full rivet pull-out" (pull-out of the deformed Ti rivet, failure mode III). (c) Force-displacement curves comparing failure modes I and III with the tensile strength of the grade 3 titanium base material rivet. (d) Relationship between the pull-out force and the "mushrooming efficiency", indicating also the failure modes for the joints

diameter (D) and the width of the deformed rivet tip (w) into a factor that gives the widening of the rivet tip as a percentage of the undeformed diameter of the rivet. This factor will be used in the following to describe the relationship between the geometry of the deformed rivet inside the composite substrate and the mechanical performance of the metallic-insert joint. It will be used to estimate the anchoring efficiency based on the area of contact between the rivet-anchoring zone and the composite. The results of the mushrooming efficiency of all of the parameter combinations are shown in Table 3. The mushrooming efficiency ranges from 34.4 % to 91.4 %.

Table 3: Summary of test results for the five parameter configurations (with three replicas for each combination), comparing joint performance and formation

Configuration	Joint performance		Joint formation		
	$F_{\text{pull-out}}$ [kN]	Failure mode	T [mm]	w [mm]	e_{mush} [%]
1	6.3 ± 0.1	III	7.4 ± 0.1	6.7 ± 0.0	34.4 ± 0.2
2	7.9 ± 0.2	III	8.1 ± 0.2	7.2 ± 0.0	43.6 ± 0.4
3	9.8 ± 0.4	III	9.4 ± 0.3	7.5 ± 0.0	50.2 ± 1.1
4	7.7 ± 0.3	III	9.1 ± 0.1	7.2 ± 0.0	44.7 ± 0.4
5	10.6 ± 0.1	I	12.9 ± 0.6	9.5 ± 0.0	91.4 ± 0.1

$$\mathrm{e_{mush}} = 100\,\frac{(w - D)}{D} \tag{1}$$

The results presented in Table 3 show that a higher mushrooming efficiency is reflected by a greater pull-out force, suggesting a correlation between them. The graph in Figure 5 d shows the relationship between the mushrooming efficiency and the pull-out force. For lower values of the mushrooming efficiency, between 30 % and 55 % (represented by red triangles), a linear relation is observed. It is also shown that these specimens failed in mode III, which is also associated with lower pull-out loads. It can also be seen that, even for very high values of the mushrooming efficiency, no significant increase of the pull-out force was achieved. Similar results have also been reported by Rodrigues et al. [38], who showed that failure of the metallic-insert joints (polycarbonate and AA2024 aluminum) under tensile loading was mainly precipitated by the

size of the anchoring feature inside the polymer substrate. Altmeyer et al. [37] demonstrated a linear relationship between the mushrooming efficiency and the pull-out force up to a threshold value of 70%, at which point the failure mode changed from mode III (pull-out of rivet) to mode I (failure of the rivet material). No further increase of the pull-out force was observed when this threshold is exceeded, explicable by the change in failure mode. When the 70% threshold for the mushrooming efficiency is exceeded, the metallic-insert joints fail in mode I, with failure taking place outside the joining region; the joint strength (pull-out force) depends only on the strength of the rivet material. Therefore, once the deformation width is large enough to lead to failure mode I, any further increase in the pull-out force can be achieved only by using a different rivet material.

3.2. Temperature evolution during joining

The base material properties of the polymer substrate and the metallic rivet affect the processing temperature. Additionally, the mechanical energy input, and thus the process parameters, are directly related to the temperature evolution during friction riveting. The temperature has been found to affect the softening and plasticizing of the components to be joined. This is expected to result in structural changes in these materials [31].

The average peak temperature generated by two of the parameter configurations in the present study were recorded using the procedure described in section 2. The measurement was carried out on the expelled composite flash. Amancio-Filiho reported in [17, 31] that, as a result of the low thermal conductivity of the polymer, the flash material has almost the same average temperature as the molten polymer layer around the plasticized rivet tip inside the polymer base plate, as discussed above. A typical thermogram extracted as a snapshot from the IR video acquired during testing is shown in Figure 6 a. The image shows the temperature distribution over the flash material expelled during the process; the location of the measurement area is highlighted.

The process parameter configurations used here were configurations 1 and

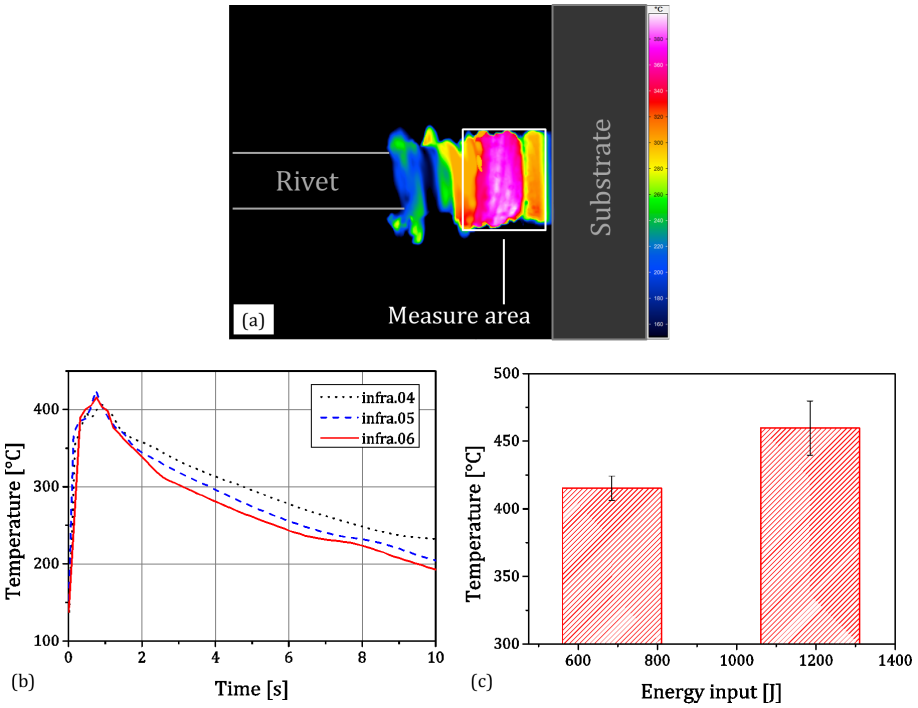

Figure 6: (a) Thermogram (IR snapshot) showing the temperature distribution of the softened PEEK composite flash material being expelled from the joining region and pushed to the surface, and the location of the measurement area. (b) Example of process temperature evolution during FricRiveting a metallic-insert joint, using configuration 1 (with high-energy input: see Table 2)

5, which were chosen because of their different energy-input levels, thus allowing the correlation to be observed between energy input and temperature evolution during the process. The mechanical energy input was calculated using equation 2, where M is the torque and ω is the angular velocity. This equation considers only the rotatory part contributing to the energy input, because the contribution of translational motion is marginal and was therefore neglected [37]. Configuration 1 represents the low energy-input level, contributing an energy input of 685 J. Configuration 5, on the other hand, represents the high-energy input level, with an energy input of 1185 J. An example of the temperature evolution during the process is shown in Figure 6 b, illustrating the temperature development over time of the three specimens joined with combination 1 parameters. The graph shows that the heating rate is very rapid, since it is related to the short friction phase of the FricRiveting process. The peak process temperature is reached after approximately 1 s, corresponding exactly to the friction time that was set for this parameter configuration. It is also shown that the temperature then decreases very slowly, which is associated with the low thermal conductivity of the PEEK composite.

$$\mathrm{E_{mech}} = \int_t M \times \omega. \tag{2}$$

The average peak temperatures and corresponding standard deviations for the two joining configurations are presented in Figure 6 c. The mean peak temperatures vary between 415 °C (for the configuration producing the lowest energy input) and 460 °C (for the combination representing the highest energy input). These temperatures exceed the PEEK composite melting temperature of 334 °C but are far below the melting temperature of the grade 3 titanium rivet (see Table 1). The highest measured temperature was less than 30 % of the melting point of the titanium; however, the temperature was probably high enough to plasticize the titanium rivet, producing an anchoring feature inside the composite substrate.

It can also be seen that higher energy input resulted in higher process tem-

peratures, which is consistent with a previous study by Amancio-Filho [17].

3.3. Characterization of the metallic-insert joint

It is known that the FricRiveting process affects the microstructure and the properties of the components to be joined [39, 37]. The microstructure and the mechanical performance of FricRiveted joints are significantly influenced by the high temperature and deformation rates involved in the joining process. These influences on both the titanium rivet and the composite substrate were investigated using a metallic-insert joint produced using configuration 5.

The microstructure was analyzed in the region of the cross-section of a metallic-insert joint. As already mentioned, the FricRiveting process rapidly deforms the tip of the titanium rivet at high temperatures to form a mushroom-shaped "head" that anchors the rivet inside the composite base plate (see Figure 7). The diameter of the rivet inside the composite increases from the initial diameter D of 5 mm to D_1 of 5.4 mm (see Figure 7) by the process known as "barreling" [40]. This deformation behavior is most likely explained as the result of applying an axial force to the rivet during FricRiveting. To gain a better understanding of the microstructural evolution taking place during the process, detailed microstructure data was taken from the different areas indicated in Figure 7.

From the analysis of the microstructural data obtained from areas 'a' to 'g', seven zones were identified in the joining region (Figure 8). The composite part consisted of the composite base material (CBM), the composite heat-affected zone (CHAZ), the composite thermomechanically affected zone (CTMAZ) and the composite stir zone (CSZ). The zones identified in the metal rivet were the metal thermomechanically affected zones 1 and 2 (MTMAZ 1 and MTMAZ 2) and the metal friction zone (MFZ). The figure shows that the boundary between MTMAZ 1 and MTMAZ 2 was V-shaped, which might be explained by the radial speed of the rivet during the process; it would be expected to be zero at the rotational axis of the rivet, and to increase outward to the circumference, generating increasing frictional heat in this direction and resulting in a higher

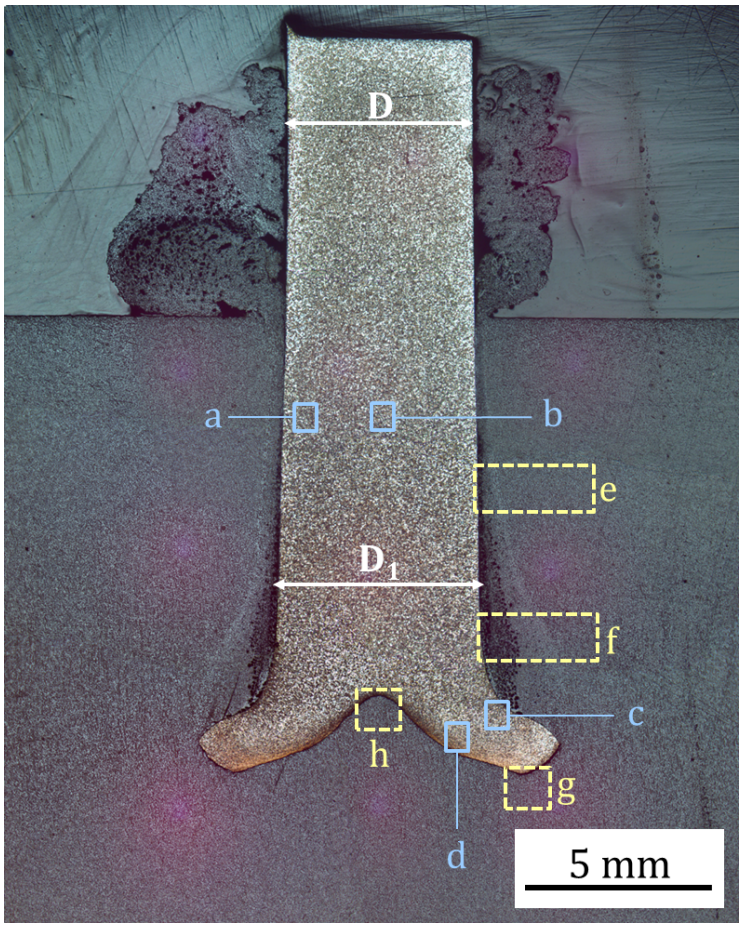

Figure 7: Macrograph of a metallic-insert joint, indicating the areas of interest (a, b, c and d in the metallic part of the joint and e, f and g in the composite part) where detailed microstructure data was acquired

temprature in the area affected by the process. Similar observations have been reported in friction welding [41], where a V-shaped border was observed between the BM and the TMAZ in an aluminum alloy 6082-T6 rod after friction surfacing on an aluminum alloy 2024-T351 substrate.

An EBSD map of the microstructure of the titanium base material is shown in Figure 3 b. The grains are colored according to their crystallographic orientation; the orientation code triangle is shown in the bottom right-hand corner. It is seen that the microstructure consists of both fine and large equiaxed titanium grains having an average grain size of approximately 22.5 µm. The structure of the base material shows a high density of HABs (95 %) and about 5% LABs. A summary of the microstructural data obtained from the titanium base material and the areas of interest (areas a to d in Figure 7) is given in Table 4.

Table 4: Average grain size and HAB proportion in the titanium base material and the different regions shown in Fgure 7

Microstructural region	Grain size [µm]	HAB fraction [%]
Base material	22.5	95
Area a	5.5	71
Area b	5.5	71
Area c	4.7	25
Area d	0.7	47

3.3.1. Areas a and b

The microstructure of area a (outer diametral region of the rivet) and b (center of the rivet) are visible in detail in Figures 9 a and b. The grain sizes and the HAB fractions are similar in both (see Table 4), which suggests that the two regions probably experienced the same amount of deformation and the same temperature. Although the parent grains in the initial microstructure of the titanium base material are still recognizable, many 85° $\langle 1\,\bar{2}\,1\,0\rangle$ twin boundaries (red lines) have formed within the grains, indicating $\{1\,0\,\bar{1}\,2\}$ $\langle 1\,0\,1\,0\rangle$ twins. Some of these 85° twin boundaries have begun to transform into random HABs due to the interaction with dislocations (e.g. those shown by black arrows) [42]. Zeng et al. [40] reported that similar twinning was predominant at deformations

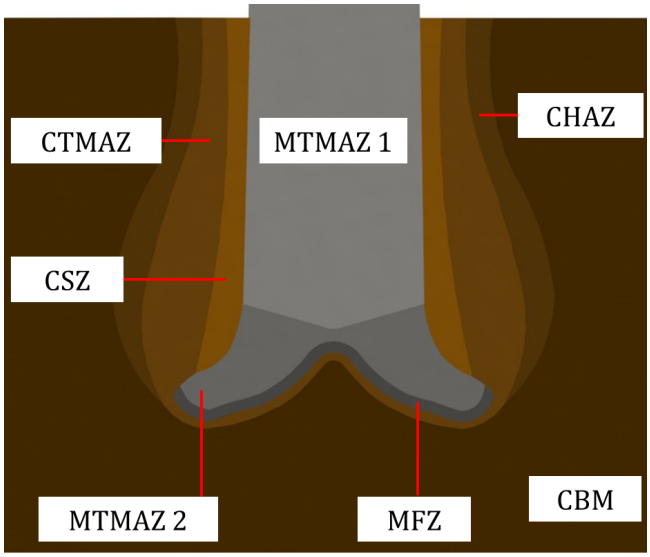

Figure 8: Schematic representation of the microstructural zones found in friction-riveted metallic-insert joints. Seven zones are indicated: composite base material (CBM), composite heat-affected zone (CHAZ), composite thermomechanically affected zone (CTMAZ), composite stir zone (CSZ), metal thermomechanically affected zone 1 (MHAZ 1), metal thermomechanically affected zone 2 (MTMAZ 2), and metal friction zone (MFZ)

up to 15 % reduction during hot compression of commercially pure titanium at temperatures to 450 °C, similar to the maximum temperature of about 460 °C measured during the friction-riveting process, as stated earlier. This type of twinning in the hexagonal structure accommodates the deformation, since such a structure lacks slip systems that usually allow the deformation to take place [43]. In addition, the fraction of the LABs was observed to increase dramatically up to 29 % due to dislocation activity. The formation of both the 85° $\langle 1\,\overline{2}\,1\,0\rangle$ twin boundaries and the LABs reflects plastic compression-related deformation in these regions. The formation of twin boundaries led to a significant decrease in average grain size, to 5.5 µm. From this data it is concluded that regions a and b may be classified as metal thermomechanically affected zones 1 (MTMAZ 1).

3.3.2. Area c

In area c the initial parent grains have been deformed in a specific direction, as shown in Figure 9 c. The formation of LAB boundaries within the grains has increased the number of LABs up to 75 %. Some of these have transformed into HABs, dividing the large grains into thinner lamellar grains (indicated by black arrows in Figure 9 c). New small grains can be seen at the boundaries of large grains, forming a "necklace" structure [42]. Most of the small grains contained an inner substructure, although small grains with no substructure were also observed. The formation of the small grains with a substructure was probably due to the gradual increase in grain-boundary reorientation. Grain-boundary bulging was also observed, leading to the formation of small grains containing no substructure, evidence that the region had been exposed to high temperatures [44]. Most of the 85° $\langle 1\,\overline{2}\,1\,0\rangle$ twin boundaries were transformed into random HABs because of the interaction with dislocations; some examples are highlighted by the red arrows in Figure 9 c [42]. Disappearance of the 85° $\langle 1\,\overline{2}\,1\,0\rangle$ twin boundaries in this way was also observed in the microstructure of hot, compressed specimens experiencing substantially high deformations and temperatures [40, 45]. The grain size in this region was reduced to 4.7 µm. The microstructural data obtained from this region is given in Table 4. These

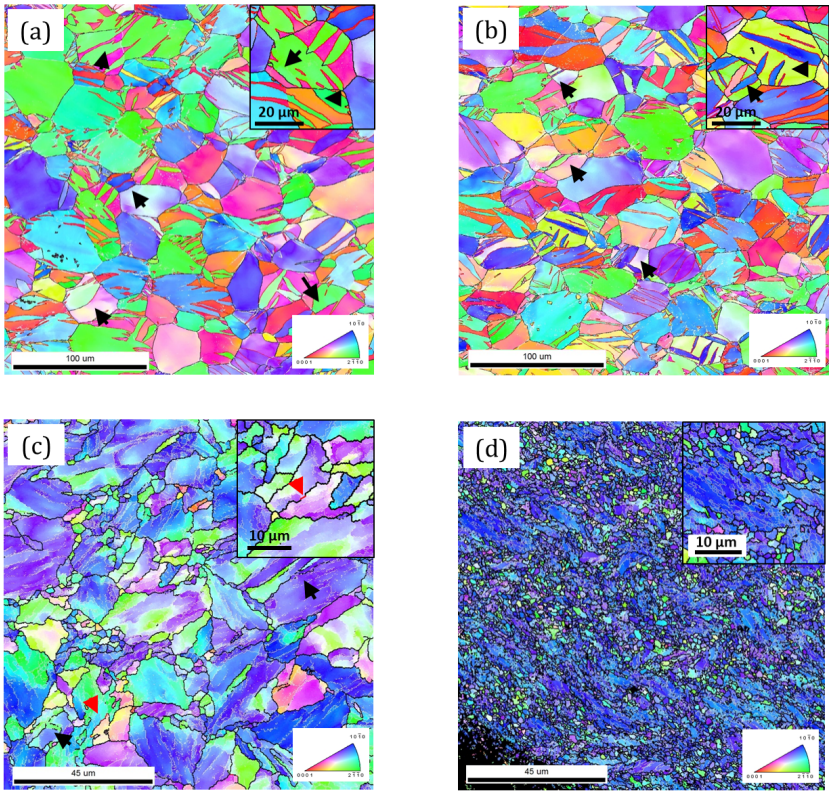

Figure 9: EBSD maps showing microstructure of regions a, b, c and d, indicating grain boundaries and their crystallographic orientation

findings are evidence that the region experienced plastic deformation due to the geometrical effect of strain and was exposed to elevated temperatures during the FricRiveting process. The analysis of this area leads to the conclusion that area c is a MTMAZ (MTMAZ 2), which is consistent with the results of previous studies [17, 18].

3.3.3. Area d

In area d, the grain structure was transformed into a new microstructure with an average grain size of about 0.7 µm (Figure 9 d). The microstructure was dominated by fine grains as well as irregular grains, shown in the magnified area at the upper right-hand corner of the figure. The high proportion of LABs (53 %) indicates that the area experienced plastic deformation, as shown in Table 4. Grain-boundary bulging can be seen, as well as small grains without LABs inside the grains, indicating that discontinuous recrystalization also took place during the FricRiveting process. The formation of a fine-grained structure is most likely due to recrystalization induced by frictional heating during the process. However, it is not clear which grain formation mechanism was dominant.

It is likely that the high temperatures were mainly caused by friction between the rivet tip and the composite substrate. On the basis of the results obtained here, this was classified as the metal friction zone (MFZ). As discussed above, the presence of the friction zone has also been proposed in the friction surfacing of an aluminum alloy 6082-T6 rod on an aluminum alloy 2024-T351 substrate [41]. Both processes are similar, in that the consumable material or rod (or rivet, in the FricRiveting case) is rotated at high speed under pressure, rubbing the substrate surface and producing frictional heating at the contact surface between the rod end (or rivet tip) and the substrate surface.

To obtain detailed insights into the evolution of the microstructure, the calculated relationship between the misorientation angle and the boundary density is shown in Figure 10. The grain-boundary density is defined as the total boundary length within the region divided by the area of the region. The large deformations and high temperatures experienced during the process generated

new high- and low-angle boundaries [42]. It was also found that the misorientation angle changed progressively from the LABs towards the HABs, as shown in Figure 10. In areas a and b, an increase in the proportion of LABs and the formation of 85° $\langle 1\,\bar{2}\,1\,0\rangle$ twin boundaries may be seen, caused by the compressive deformation induced by the axial force applied to the rivet, as mentioned earlier. In area c, the number of LABs and HABs increased greatly at the same time as the 85° $\langle 1\,\bar{2}\,1\,0\rangle$ twin boundaries vanished. This kind of change was mainly due to the interaction of the boundaries with the dislocations caused by the geometrical effect of strain induced by the forged mushroom-shaped head on the rivet. In area d, the number of boundaries progressively increased, as shown in Figure 10. It is likely that this phenomenon is related to the formation of deformation-induced boundaries and the subsequent accumulation of misorientation angles. Previous studies on friction stir welding and friction surfacing of aluminum alloys [41] have interpreted progressive boundary movement like this in terms of continuous rather than discontinuous recrystalization. From the present data, it is evident that continuous recrystalization plays an important role in the development of the microstructure of the rivets during the FricRiveting process.

3.3.4. Areas e and f

The microstructure of area e located at the upper and lower regions adjacent to the metallic rivet (see Figure 7) is shown in Figure 11 a. From the morphology of the PEEK composite (porosity fraction and fiber orientation), areas e and f (Figure 11 a and b) have been further subdivided into the four regions 1 to 4. The formation of the porosity in the PEEK is probably due to its thermal degradation [17, 18] following exposure to temperatures up to approximately 450 °C, which is above its melting point (T_m) of the PEEK.

An enlarged map of region 1 (indicated in Figure 11 a and b) is shown in Figure 12 a. The porosity fraction in this region is higher than in the other three regions. Most of the fibers in this region 1 have been realigned into one direction. It is seen in Figure 12 b that the fibers appear as circular dots, indicating that

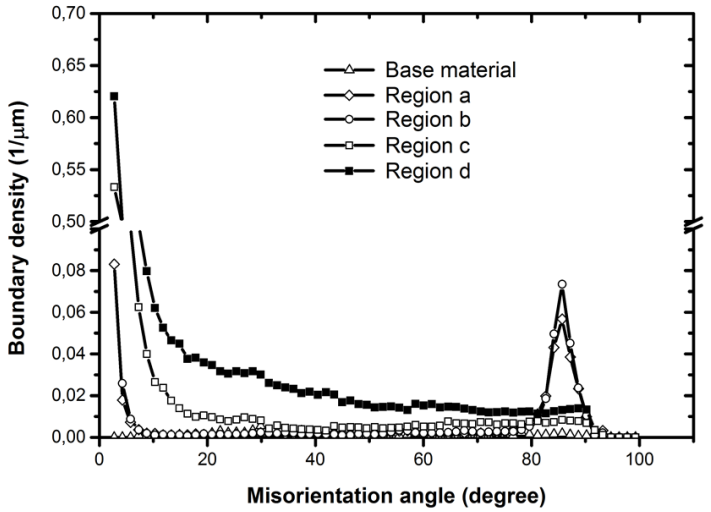

Figure 10: Grain boundary densities calculated for the base material and areas a, b, c and d

they are oriented in a direction normal to the observation plane. This indicates that material flowed in a circular movement around the rivet (stirring), causing the fibers to be realigned parallel to the rivet as it rotated; region 1 has been strongly affected by the rotation of the rivet in this way.From this evidence, region 1 was classified as the composite stir zone (CSZ). It should be noted that, although the PEEK had been altered significantly in this region, there was no evidence in Figure 11 of the significant changes to the microstructure of the rivet itself at area a that were seen in area d following severe deformation of the rivet. This is an indication that the main frictional heat was not generated at the surface of the cylindrical part of the rivet during the process.

An enlarged image of region 2 (see Figure 11) is shown in Figure 12 c. In this region, the porosity fraction is lower than in the CSZ (region 1), indicating that the composite experienced lower temperatures here than in the CSZ. It is also seen that the fibers have been reorientated and are aligned such that they are seen in the cross-section as elliptical dots. The elliptical shape is the result of helical realignment as shown in Figure 12 d. Two factors may have

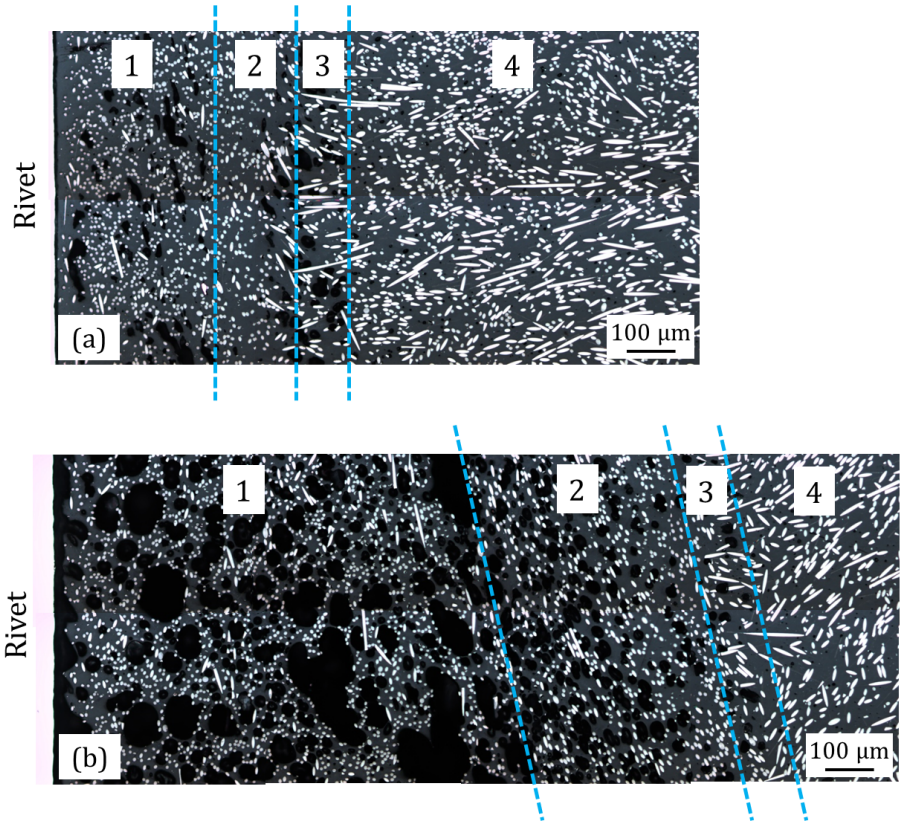

Figure 11: Micrograph with higher magnification of (a) area e and (b) area f, located in Figure 7

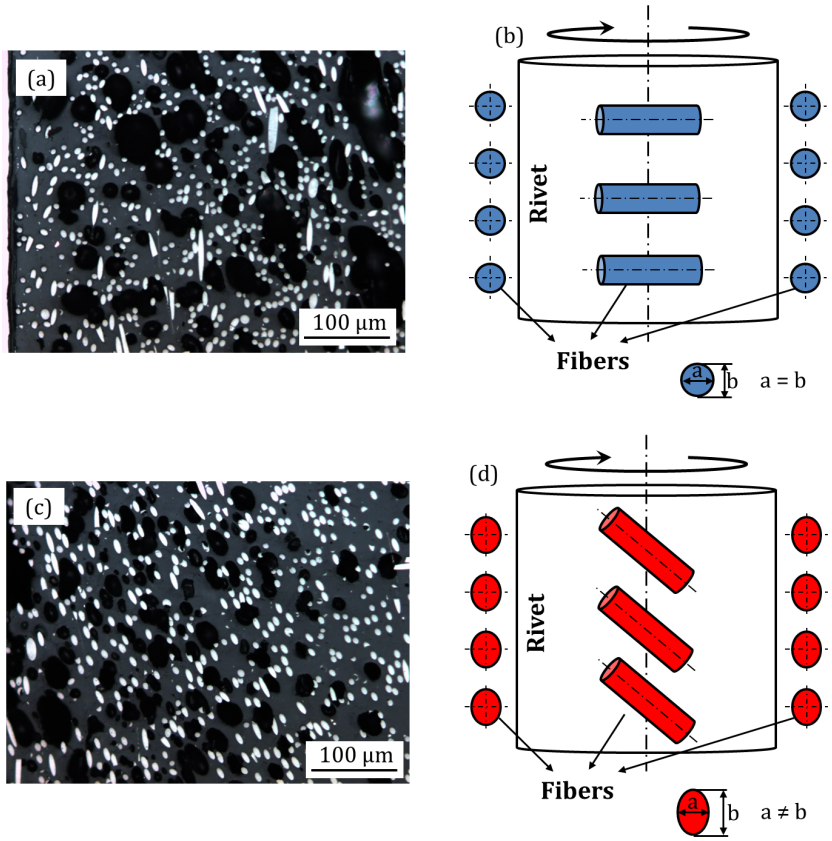

Figure 12: Composite stir zone (CSZ): (a) Enlarged image of region 1 identified in Figure 11. (b) Schematic of the fiber orientation in this region; composite thermomechanically affected zone (CTMAZ). (c) Enlarged image of region 2 in Figure 11. (d) Schematic of the fiber orientation in this region

been responsible for this form of fiber orientation: rotation of the rivet, and upward movement of the softened composite being suppressed by the rivet. First, rotation caused the fibers to move around the rivet and take on a new alignment, as for the CSZ but to a lesser extent, since this region is further from the rotating rivet. Second, the upward flow of the softened composite was suppressed when the rivet penetrated the substrate. The combination of these two factors led to the fibers' being tilted (Figure 12 d). This is evidence that region 2 experienced high temperatures and large deformation, and it was therefore classified as a composite thermomechanically affected zone (CTMAZ). The presence of this zone was reported, but without evidence, by Amancio-Filho [17, 18].

Comparing Figures 11 a and b, it is seen that both the CSZ and the CTMAZ in area f (Figure 11 b) are broader than in area e (Figure 11 a). This is possibly due to the differences in temperature experienced by the two areas. It is believed that the temperature was higher in area f than in area e, since it is likely that most of the heat was generated by friction between the tip of the rivet and the composite. Material closest to the heat source at the rivet tip would therefore be expected to show evidence that it was the largest heat-affected zone.

Region 3, located between regions 2 and 4, was very narrow (Figure 13 a). The presence of pores indicated that, although the region had been exposed to elevated temperatures, the porosity fraction was much lower than in the CTMAZ and CSZ. The temperature affecting this region was considerably lower than in the regions discussed above. The fiber orientation shown in Figure 13 a differs from both the CSZ and CTMAZ, and appears to be similar to the base material. This implies that the fiber orientation in region 3 was not affected by either the rotation of the rivet or the upward flow of the softened composite. Since only the matrix of the composite was affected by the elevated temperatures as evidenced by the pores present in the microstructure, region 3 is classified as the composite heat-affected zone (CHAZ).

Figure 13 b is an enlarged micrograph of region 4 microstructure showing that the fraction of pores is minimal, and is comparable to the microstructure

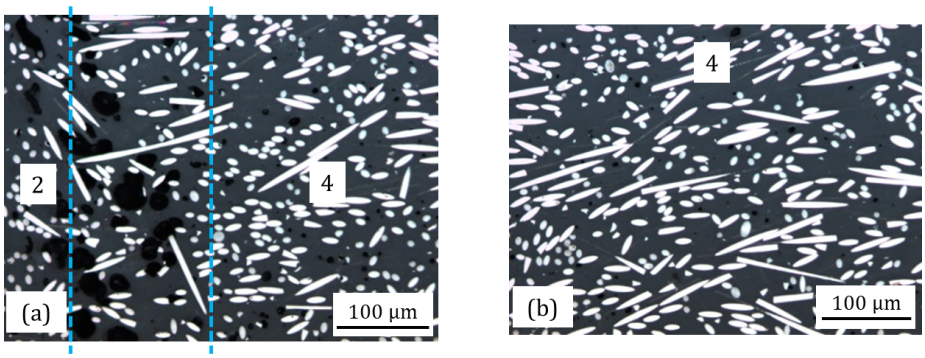

Figure 13: Enlarged map of region 3, the composite heat-affected zone (CHAZ), and region 4, the PEEK composite base material (CBM). Locations of the two regions are shown in Figure 11 a and b

of the PEEK composite base material. Thus region 4 was classified as composite base material (CBM).

3.3.5. Areas g and h

To better understand the composite microstructure immediately beneath the rivet, areas g and f in Figure 7) were chosen. A gap can be seen in both areas between the rivet and the PEEK composite (indicated by a red arrow in Figure 14 a and red broken lines in Figure 14 b. The gap is probably due to contraction (shrinkage) of the cooling rivet.

From the morphology of the PEEK composite, in particular the fiber orientation, each area was subdivided into two regions (regions 2 and 4). In region 2, the fibers have been reorientated, probably due to material flow during the joining process. In area g, most of the fibers are seen to be aligned almost horizontally, or parallel to the rivet surface. In region 2 of area h, most of the fibers have been reorientated in a direction perpendicular to the observation plane. In both areas g and h, the porosity densities in regions 2 and 4 are identical. From this information, the evolution of the PEEK composite microstructure may be explained as follows.

As mentioned above, reorientation and alignment of the fibers probably occurred with material flow in this region; this also required a plasticized matrix.

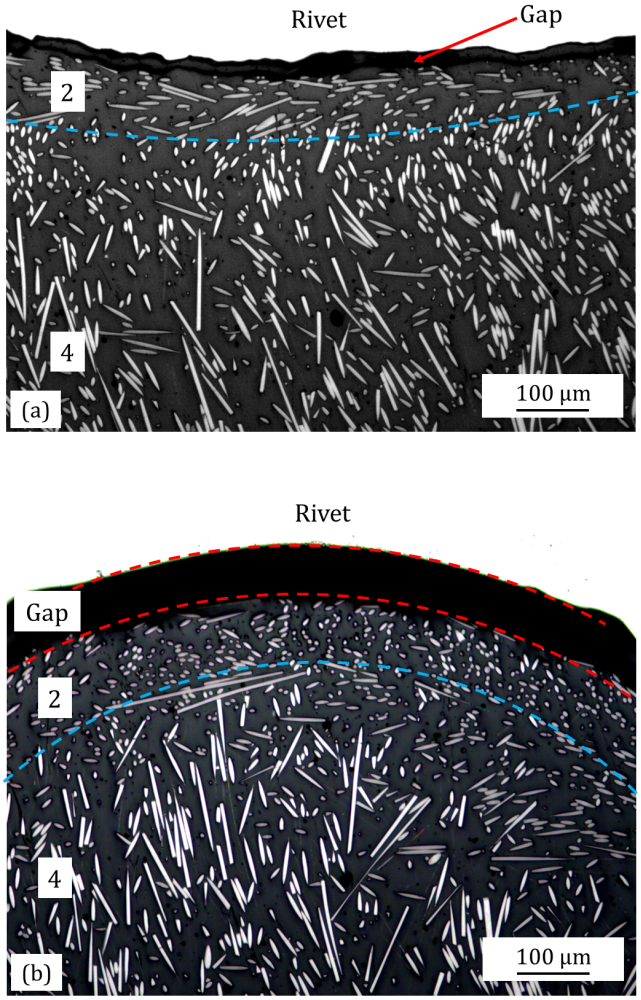

Figure 14: Higher-magnification micrograph of areas g and h under the deformed rivet tip, located where shown in Figure 7

The fibers were aligned almost horizontally in region 2, consistent with outward flow of the softened polymer during the forging step. The fibers are seen to be long and elongated, but they differ in appearance from those aligned parallel to the rivet. The reorientation in this case occurred as a result of both rotation and penetration of the rivet. During the forging step, the axial force applied to the rivet increased as rotation speed decreased, causing the material to flow outwards. This also explains the narrow region 2 thermomechanically affected zone and the lack of porosity due to polymer degradation within the composite, similar to that observed in areas e and f. These findings demonstrate that region 2 was exposed to elevated temperatures and experienced deformation; thus it was classified as CTMAZ [17, 18].

In region 2 of area h (Figure 14 bb), the fibers were reorientated and realigned as a result of the material flow. The orientation appears to be almost perpendicular to the observation plane. The fibers in the cross-sectional view resemble elliptical dots. Unlike region 2 of area g, however, the material is believed to have been only slightly affected by outward material flow, since it was trapped in the bell-shaped pocket created at the center of the rivet tip by the forging action, and the fibers were tilted as shown in Figure 12 d. This indicates that region 2 was exposed to high temperatures and was considerably deformed; it was also characterized as CTMAZ [17, 18].

In areas g and h, region 4 was located beneath region 2. There is no evidence that region 4 contained more pores than the CBM (see Figure 13 b), or that fibers had been reorientated. These together indicate that region 4 in areas g and h was neither heated to elevated temperatures nor deformed, and was therefore classified as CBM.

3.3.6. Material flow

As mentioned earlier, although the tip of the rivet was severely deformed and was exposed to high temperatures, the polymer at the interface was not altered to any great extent. However, the composite material in contact with the rotating rivet was thermally degraded, as evidenced by an increased porosity

ratio.To better understand this, it was important to study the material flow of the composite during the FricRiveting process.

The frictional heat generated by the the tip of the rotating rivet interacting with the composite material softened the matrix of the composite; the centrifugal force generated by the rotation together with the applied axial force caused the softened material to flow around the rivet. As the rotating rivet penetrated the composite substrate, its tip deformed until it assumes the desired mushroom-like shape. The penetration also caused the softened composite to flow toward the substrate surface. The fibers in the composite matrix were reorientated and, due to their very high aspect ratio, were aligned parallel to the material flow. The extent of material flow and fiber reorientation varied depending on the distance from the rotating rivet. From this information, the material flow with respect to fiber reorientation has been summarized in Figure 15, in which the blue-colored fibers are in the CSZ and the red-colored fibers are in the CTMAZ.

4. Conclusion

The present study examined the mechanical performance and the microstructure of friction-riveted metallic-insert joints made of PEEK composite reinforced with 30 % short carbon fibers and grade 3 titanium. The results led to the following conclusions:

- The manufacture of high-strength friction-riveted metallic-insert joins was achieved. The specimens produced using the parameter configuration 5 (RS: 20000rpm, FT: 1.5 s, FP: 0.8 MPa, FoP: 1 MPa and FoT: 10 s) produced an average pull-out force of 10.6 kN, which corresponds to the base material strength of the grade 3 titanium rivet.

- Higher energy input produced higher process temperatures. The average peak temperature of the configuration with the highest energy input was 460 °C, which is less than 30% of the melting point of the grade 3 titanium rivet but sufficient to plasticize the rivet tip inside the composite substrate.

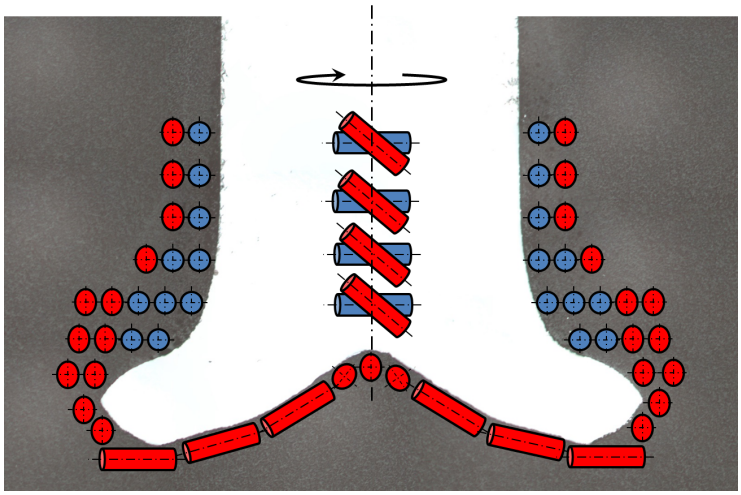

Figure 15: Material flow during FricRiveting. Blue fibers indicate material flow in the CSZ; red fibers indicate flow in the CTMAZ

- The high temperature and deformation rates resulted in several microstructural changes in the titanium rivet and in the composite substrate, creating different thermally and thermomechanically affected zones in the vicinity of the join. Microstructural analysis enabled seven microstructural zones to be classified in the joining area: the composite base material (CBM), a composite heat-affected zone (CHAZ), a composite thermomechanically affected zone (CTMAZ), a composite stir zone (CSZ), two metal thermomechanically affected zones (MHAZ 1 and MTMAZ 2) and a metal friction zone (MFZ).

- The orientation of the constituent fibers of the composite was successfully used to determine the flow behavior of the composite material when it was heated by the friction riveting process in the vicinity of the rotating titanium rivet.

Reference

[1] HP Zepf. *Faserverbundwerkstoffe mit thermoplastischer Matrix*, volume 529 of *Kontakt & Studium*. Expert-Verlag, Renningen-Malmsheim, 1997.

[2] S. T. Peters. *Handbook of Composites*. Chapman & Hall, London, second edition edition, 1998.

[3] Jr Robert W. Messler. *Joining Composite Materials and Structures*, pages 647–696. Butterworth-Heinemann, Burlington, 2004. doi: DOI: 10.1016/B978-075067757-8/50014-2.

[4] VV Vasiliev and EV Morozov. *Mechanics and Analysis of Composite Materials*. Elsevier Science Ltd., Oxford, 2001.

[5] V. K. Stokes. Joining methods for plastics and plastic composites: An overview. *Polymer Engineering and Science*, 29(19):1310–1324, 1989. 10.1002/pen.760291903.

[6] D. M. Maguire. Joining thermoplastic composites. *SAMPE Journal*, 25(1):11–14, 1989.

[7] R Rudolf, P Mitschang, M Neitzel, and C Rueckert. Welding of high-performance thermoplastic composites. *Polymer and Polymer Composites*, 7(5):309–315, 1999.

[8] Ali Yousefpour, Mehdi Hojjati, and Jean-Pierre Immarigeon. Fusion bonding/welding of thermoplastic composites. *Journal of Thermoplastic Composite Materials*, 17(4):303–341, 2004.

[9] ST Amancio-Filho and JF dos Santos. Joining of polymers and polymer-metal hybrid structures: Recent developments and trends. *Polymer engineering and Science*, 49:1461–76, 2009.

[10] Jr Robert W. Messler. The challenges for joining to keep pace with advancing materials and designs. *Materials & Design*, 16(5):261–269, 1996.

[11] T. J. Ahmed, D. Stavrov, H. E. N. Bersee, and A. Beukers. Induction welding of thermoplastic composites–an overview. *Composites Part A: Applied Science and Manufacturing*, 37(10):1638–1651, 2006. doi: DOI: 10.1016/j.compositesa.2005.10.009.

[12] D. Stavrov and H. E. N. Bersee. Resistance welding of thermoplastic composites-an overview. *Composites Part A: Applied Science and Manufacturing*, 36(1):39–54, 2005. doi: DOI: 10.1016/j.compositesa.2004.06.030.

[13] Wolfgang Knapp, S. Clement, C. Franz, M. Oumarou, and J. Renard. Laser-bonding of long fiber thermoplastic composites for structural assemblies. *Physics Procedia*, 5, Part B(0):163–171, 2010.

[14] S Amancio, M Beyer, and JF dos Santos. Verfahren zum Verbinden eines metallischen Bolzens mit einem Kunststoff-Werkstück, 2006.

[15] ST Amancio-Filho, M Beyer, and JF dos Santos. Method of connecting a metallic bolt to a plastic workpiece, 2009.

[16] ST Amancio-Filho and JF dos Santos. Fricriveting: a new technique for joining thermoplastics to lightweight alloys. In *Materials Science and Technology (MS&T)*, 2008.

[17] ST Amancio-Filho. *Friction Riveting: development and analysis of a new joining technique for polymer-metal multi-materials structures.* Dissertation, 2007.

[18] ST Amancio-Filho. Friction riveting: development and analysis of a new joining technique for polymer-metal multi-material structures. *Welding in the World*, 55(01 02):13 – 24, 2011.

[19] L Blaga, R Bancila, JF dos Santos, and ST Amancio-Filho. Friction riveting of glass-fibre-reinforced polyetherimide composite and titanium grade 2 hybrid joints. *Materials and Design*, 50:825–829, 2013.

[20] Fengying Yao, Jun Zheng, Mingbi Qi, Wei Wang, and Zongneng Qi. The thermal decomposition kinetics of poly(ether-ether-ketone) (peek) and its carbon fiber composite. *Thermochimica Acta*, 183(0):91–97, 1991. doi: 10.1016/0040-6031(91)80448-R.

[21] Robert Maksimov and Josef Kubat. Time and temperature dependent deformation of poly(ether ether ketone) (peek). *Mechanics of Composite Materials*, 33(6):517–525, 1997.

[22] Ajit Kumar Mishra and Jerold M. Schultz. Kinetics of strain-induced crystallization during injection molding of short fiber composites of poly(ether ether ketone). *Polymer Composites*, 12(3):169–178, 1991.

[23] Francisco Mata, V. N. Gaitonde, S. R. Karnik, and J. Paulo Davim. Influence of cutting conditions on machinability aspects of peek, peek cf 30 and peek gf 30 composites using pcd tools. *Journal of Materials Processing Technology*, 209(4):1980–1987, 2009. doi: 10.1016/j.jmatprotec.2008.04.060.

[24] C.A. Harper. *Handbook of plastics, elastomers & Composites.* McGrawHill Handbooks, 2002.

[25] *Polymer Data Handbook.* OxButterworth-Heinemann, Inc., 1999.

[26] J.A. Brydson. *Plastic Materials.* Butterworth-Heinemann, 1999.

[27] Ketron PEEK. Technical report, Arthur Krüger Technik in Kunststoffen.

[28] E.W. Collings R. Boyer, G. Welsch. *Materials properties handbook: Titanium alloys.* ASM International, 1998.

[29] J.C. Williams G. Lütjering. *Titanium*. Springer-Verlag Berlin Heidelberg, 2007.

[30] U. Zwicker. *Titan und Titanlegierungen*. Springer-Verlag, Berlin Heidelberg New York, 1974.

[31] ST Amancio and JF dos Santos. FricRiveting: A new joining technique for thermoplastics-lightweight alloy structures. *Materials Science and Technology*, pages 2362 – 2373, 2008.

[32] DIN Deutsches Institut für Normung e.V. Radiographic testing of welded joints, 2002.

[33] DIN Deutsches Institut für Normung e.V. Elektrische und optische verbindungselemente, 1992.

[34] G.F. Vander Voort. *Metallography priciples and practice*. Number ISBN-13: 978-0-87170-672-0. ASM International, 1999.

[35] G. Petzow. *Metallographisches keramographisches plastographisches Ätzen*. Gebrüder Borntraeger, Berlin Stuttgart, 1994.

[36] V. Ventzke S. Amancio, J. dos Santos. Determination of fracture mechanisms under tensile loading in a commercial available engineering thermoplastic material joined by fricriveting, 7-11 September 2008 2008.

[37] J Altmeyer, JF dos Santos, and ST Amancio-Filho. Effect of the friction riveting process parameters on the joint formation and performance of ti alloy/short-fibre reinforced polyether ether ketone joints. *Materials & Design*, 60(0):164 – 176, 2014.

[38] CF Rodrigues, LA Blaga, JF dos Santos, LB Canto, E Hage Jr., and ST Amancio-Filho. Fricriveting of aluminum 2024-t351 and polycarbonate: Temperature evolution, microstructure and mechanical performance. *Journal of Materials Processing Technology*, (0):–, 2014.

[39] ST Amancio-Filho, J Roeder, SP Nunes, JF dos Santos, and F Beckmann. Thermal degradation of polyetherimide joined by friction riveting (fricriveting). part i: Influence of rotation speed. *Polymer Degradation and Stability*, 93(8):1529–38, 2008.

[40] Zhipeng Zeng, Stefan Jonsson, and Hans JÃ¸rgen Roven. The effects of deformation conditions on microstructure and texture of commercially pure ti. *Acta Materialia*, 57(19):5822–5833, 2009. doi: DOI: 10.1016/j.actamat.2009.08.016.

[41] U Suhuddin, S Mironov, H Krohn, M Beyer, and JF dos Santos. Microstructural evolution during friction surfacing of dissimilar aluminum alloys. *METALLURGICAL AND MATERIALS TRANSACTIONS A*, 43A:5224–31, 2012.

[42] S. Mironov, Y.S. Sato, and H. Kokawa. Development of grain structure during friction stir welding of pure titanium. *Acta Materialia*, 57(15):4519 – 4528, 2009.

[43] Valerie Randle Olaf Engler. *Introduction to Texture Analysis: Macrotexture, Microtexture, and Orientation Mapping*. CRC Press, 2009.

[44] S Mironov, YS Sato, H Kokawa, H Inoue, and Tsuge S. Structural response of superaustenitic stainless steel to friction stir welding. *Acta Materialia*, 59:5472–5481, 2011.

[45] J.C. Williams, R.G. Baggerly, and N.E. Paton. Deformation behavior of hcp ti-al alloy single crystals. *Metallurgical and Materials Transactions A*, 33(3):837–850, 2002.